Electronic Supplementary Material (ESI) for Energy & Environmental Science.

Supporting information

Ultra-long-life and highly reversible Zn metal anodes enabled by a desolvation and deanionization interface layer

Xiaotan Zhang, Jiangxu Li, Dongyan Liu, Mengke Liu, Tiansheng Zhou, Kaiwen Qi, Lei Shi, Yongchun Zhu,* and Yitai Qian*

Department of applied Chemistry,

University of Science and Technology of China, Hefei, Anhui, 230026, China

Corresponding authors:

ychzhu@ustc.edu.cn

ytqian@ustc.edu.cn

Theoretical Calculations.

Based on the density function theory (DFT),[1,2] the first-principles calculations have been performed to investigate the adsorption behaviors on CNWs, GN and CNG by Vienna Ab-initio Simulation Package (VASP).[3,4] For the periodic DFT calculations, we chose the projector-augmented-wave (PAW)[5] pseudopotentials and Perdew-Burke-Ernzerhof (PBE) exchange correlation functionals.[6] The planewave basis cutoff energy of 500 eV was used for the self-consistent field method with an electronic energy convergence of 1005 eV/atom, while the 3×3×1 k-point samplings are used within the Γ center Monkhorst-Pack scheme. For the lattice constants optimization and structure relaxations, the remanent Hellmann-Feynman forces were less than 0.01 eV/Å. For the van der Walls forces, we used the DFT-D3[7] method of Grimme to get an accurate description of this force. Furthermore, we also used the density functional molecular dynamics (DFTMD) to simulate the dynamical process of hydrated zinc ions $[Zn(H_2O)_6]^{2+}$ on the surface of CNWs.

The CNWs structure has been studied for a long time. Both I_α and I_β structures can exist in CNWs.[8,9] Considering the X-ray diffraction pattern of cellulose in our experiment, we use I_β CNWs for our following calculations. The I_β CNWs was constructed by our experimental data and the information published by Nishiyama et al.[9] First, we focused on the adsorption process of CNWs and graphene. The surface model for cellulose and graphene has been constructed and we used 12 Å vacuums to eliminate the interaction between surfaces. Due to the configurations of those surfaces, we set H_2O, Zn^{2+} and $[Zn(H_2O)_6]^{2+}$ on different surface positions(such as hollow, bridge and top positions of different atoms) to get the most stable states, respectively. The adsorption energy can be defined as:

$$E_{ad} = E_{tot} - E_{base} - E_{mol} \quad (1)$$

Where E_{ad}, E_{tot}, E_{base}, and E_{mol} denote the adsorption energy, the total energy of adsorption models, the energy of the matrix such as graphene or CNWs and the energy of the adsorption molecules such as H_2O, Zn^{2+} and $[Zn(H_2O)_6]^{2+}$.

The interface energy of CNWs and graphene can be obtained as:

$$\gamma = \frac{E_{CNG} - E_{CNWs} - E_{GN}}{A} \quad (2)$$

E_{CNG} is the total energy of CNG interface model. E_{CNWs} is the total energy of the CNWs's surface model and E_{GN} is the energy of graphene. A is the area of the interface.

As shown in Figure M1, the temperature of the simulated environment always maintained at 300K. During the MD simulation, the energy of the whole system and the average coordination number

(ACN, Figure M2) of hydrated Zn^{2+} decreased consistently, demonstrating the desolvation effect of CNWs, where the corresponding ACN of hydrated Zn^{2+} was 4.8 (from 0 to 2000 steps) and 3.2 (from 2000 to 10000 steps), respectively.

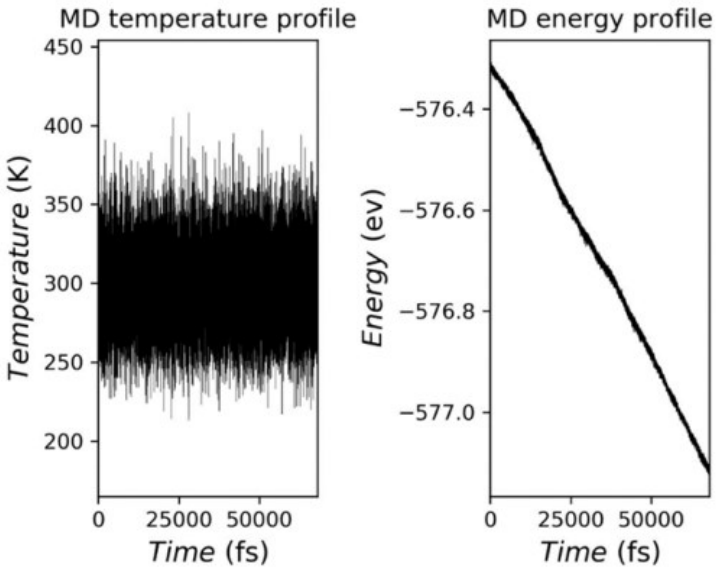

Figure M1. Temperature and energy along with time in the MD simulation of the desolvation process of CNG membrane.

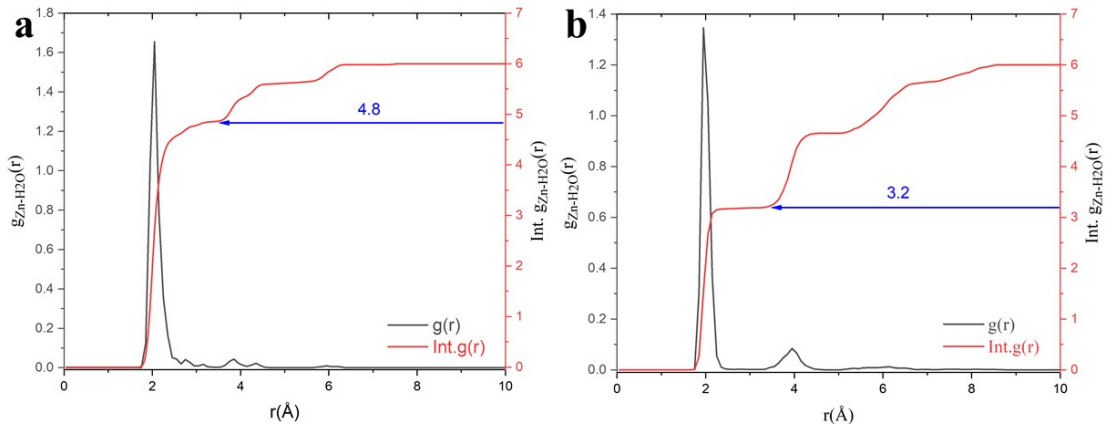

Figure M2. Zn-H_2O radial distribution function calculated using DFT-D3 function at the MD modeling of 300K. Time step from (a) 0 to 2000 and (b) 2000 to 10000.

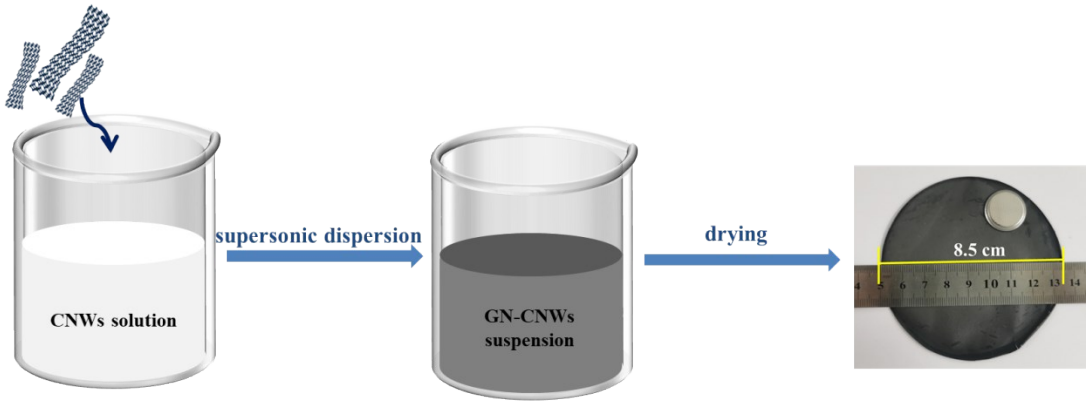

Figure S1. Schematic illustration of fabrication procedure for CNG membrane.

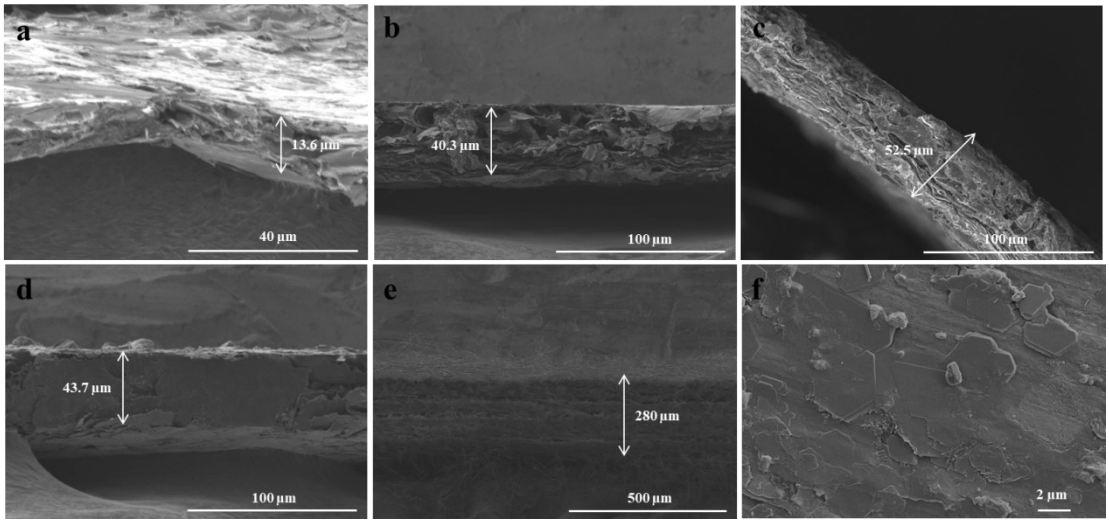

Figure S2. Cross-sectional images of CNG membranes with different thickness. (a) CNG-1, (b) CNG-2, (c) CNG-3 before and (d) after compression process, (e) glass fiber separator. (f) Zn deposition morphology on CNG-1/Zn anode after 15mins.

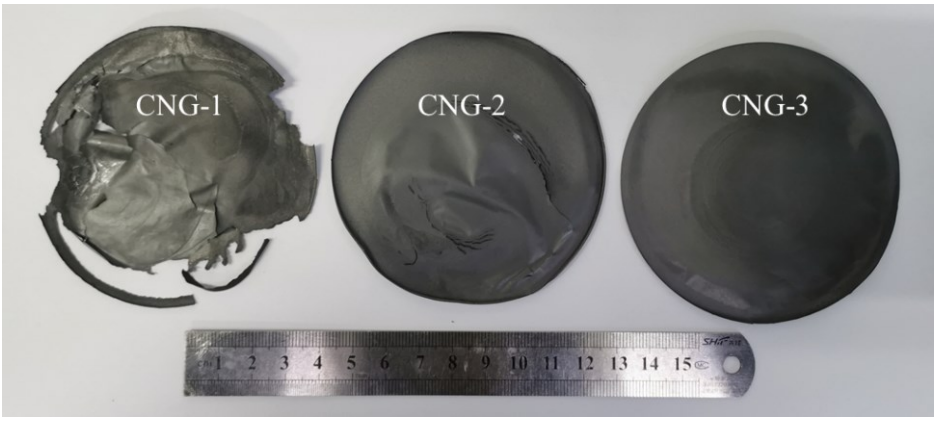

Figure S3. Macroscopic image of CNG membranes.

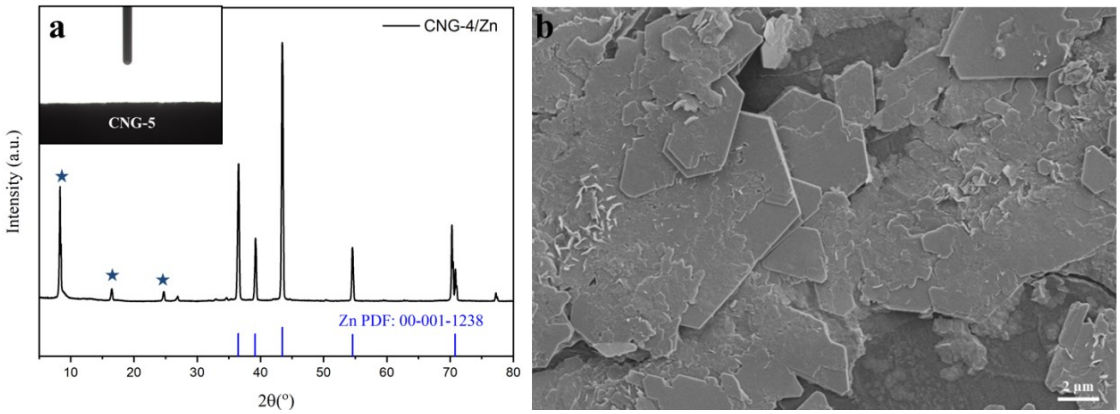

Figure S4. (a) XRD analysis of Zn foil with CNG-4 layer after 15 mins deposition (the inset image is WCA of CNG-5). (b) SEM image of Zn anode protected by CNG-5 membrane after plating 15 mins. Current density, $J = 4$ mA cm^{-2}.

At the experimental design stage, we prepared CNG membranes with different thicknesses by regulating the mass of graphene, where the mass ratio of graphene and CNWs was fixed at 1:1, as shown in Table S1. The thickness of CNG membranes are 13.6 (CNG-1, Figure S2a), 40.3 (CNG-2, Figure S2b), and 52.5 μm (CNG-3, Figure S2c), respectively. We chose CNG-3 membrane as the interface layer for three reasons: (i) due to the difficulty of preparation process, it is difficult to obtain a complete and uniform CNG membrane if the thickness decreases (Figure S3); (ii) although the thickness of the layered CNG-3 membrane is nearly 52.5 μm, the actual thickness is 43.7 μm (Figure S2d) after being compressed during the battery assembly process, which is much less than that of glass fiber separator (280 μm, Figure S2e); (iii) the Zn deposition morphology does not change when using CNG-1 membrane, as shown in Figure S2f. Therefore, with the decrease in the thickness of CNG membrane, Zn deposition morphology will not be influenced. So the CNG-3 membrane ($m_{graphene}$: m_{CNWs}=1:1, $m_{graphene}$ = 120 mg) was selected to induce Zn redirected electrodeposition for the experimental consistency.

Besides, the CNG membranes with three different mass ratios (1:2, 1:1, and 2:1) of hydrophobic graphene and hydrophilic CNWs were prepared, where the graphene mass was fixed (Table S2). For CNG-4 membrane, the water contact angle was ≈0° (inset image of Figure S4a). The excellent super-hydrophilicity of the interface layer is not favorable to screen H_2O molecules, causing Zn anode corrosion (Figure S4a). But for CNG-5 membrane, the electrical conductivity of CNG membrane was improved due to the reduction of CNWs mass, which caused Zn^{2+} deposition on the surface of CNG-5 membrane (Figure S4b). Because an ideal interface layer should possess high ionic conductivity and low electrical conductivity, thus the CNG-3 membrane ($m_{graphene}$: m_{CNWs}=1:1,

$m_{graphene}$ = 120 mg) was considered to be the best one to perform a series of experiments.

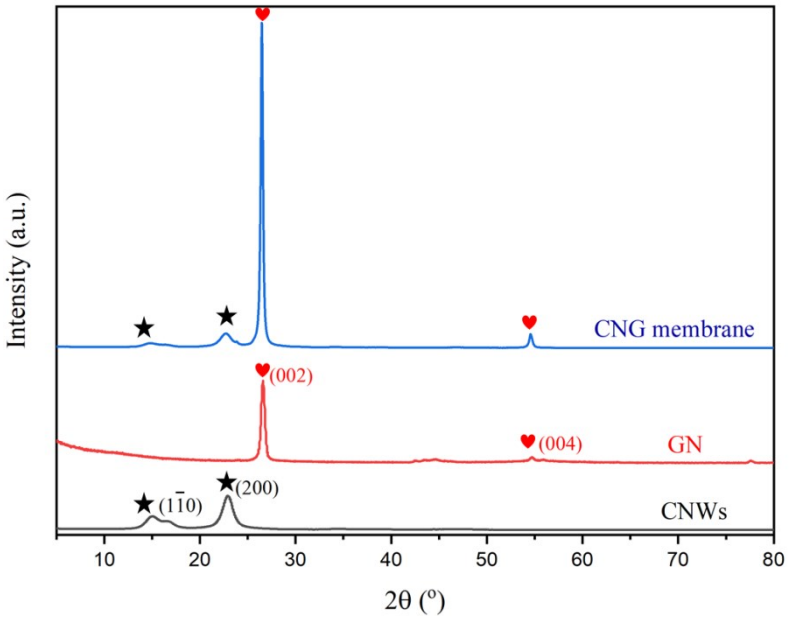

Figure S5. XRD patterns of CNWs, GN, and CNG membrane.

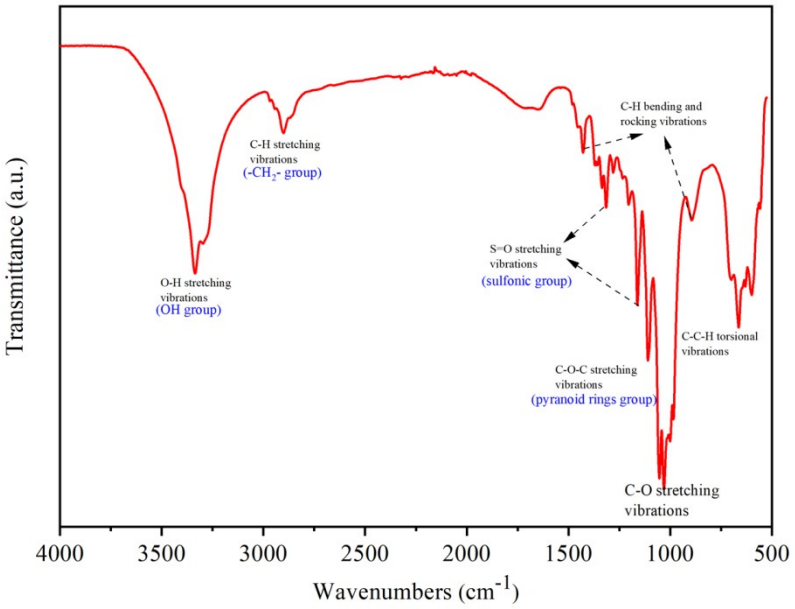

Figure S6. FT-IR spectra of CNWs.

The broad peak located at 3,344-3,415 cm^{-1} region is attributed to stretching and bending vibrations of OH group. The adsorption at ≈2912, 1140 and 1079 cm^{-1} is related to the stretching vibrations of C-H (-CH_2- group), C-O-C (pyranoid rings group) and C-O, respectively. The peaks at

1367 cm^{-1} and 1170 cm^{-1} represent the stretching vibrations of S=O (sulfonic group).

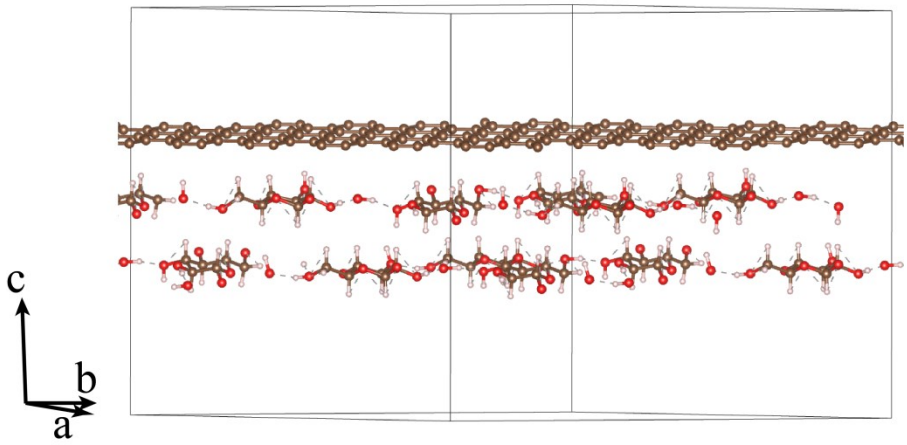

Figure S7. The interface energy of CNWs and GN was calculated by DFT simulation.

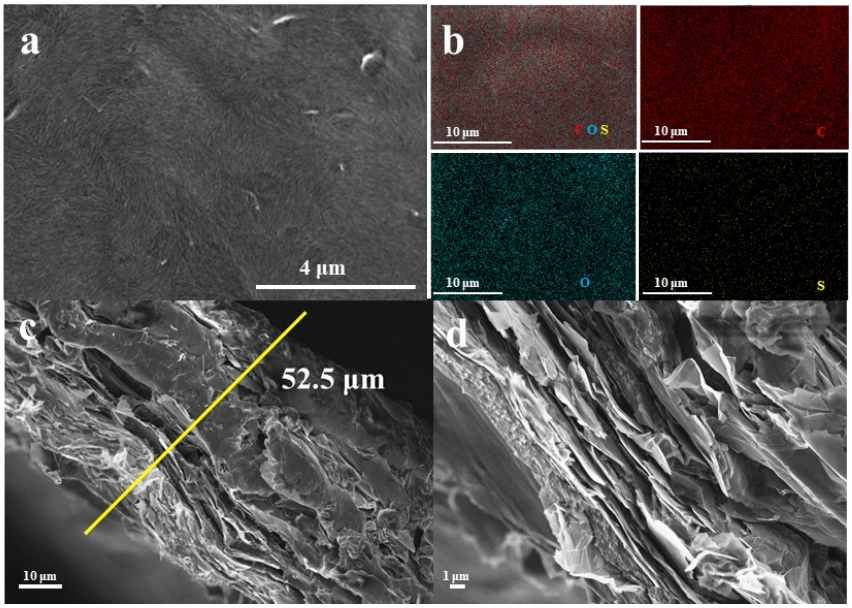

Figure S8. Morphological characterizations of CNG membrane. (a) FE-SEM, (b) EDS and (c, d) cross-sectional images of CNG.

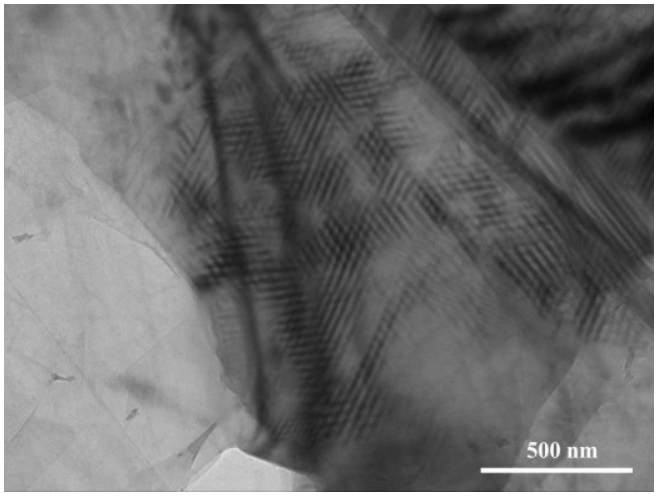

Figure S9. TEM image of CNG membrane.

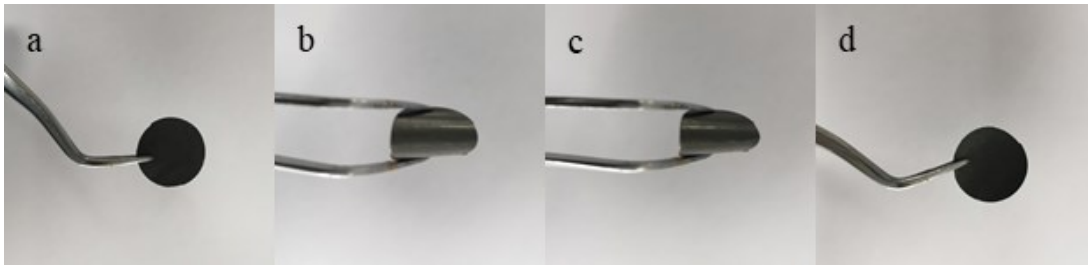

Figure S10. Flexible bending test. Photograph of (a) the initial CNG membrane, (b, c) the bending CNG membrane. (d) the CNG membrane after experiment.

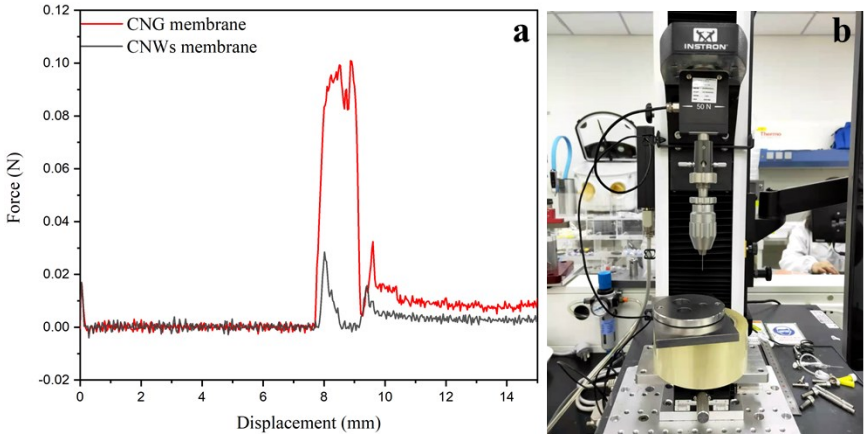

Figure S11. Penetration force-displacement curve of CNG membrane and CNWs membrane.

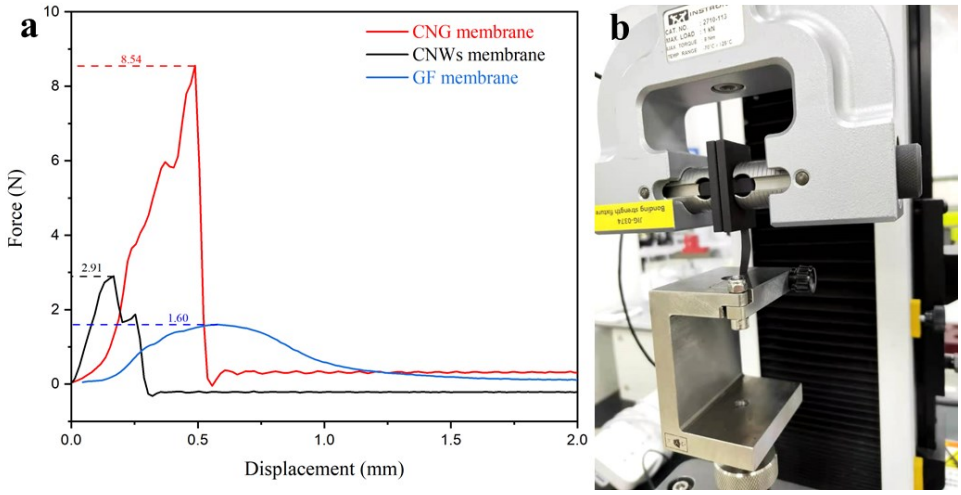

Figure S12. Load-deformation curve of CNG membrane, CNWs membrane, and GF membrane.

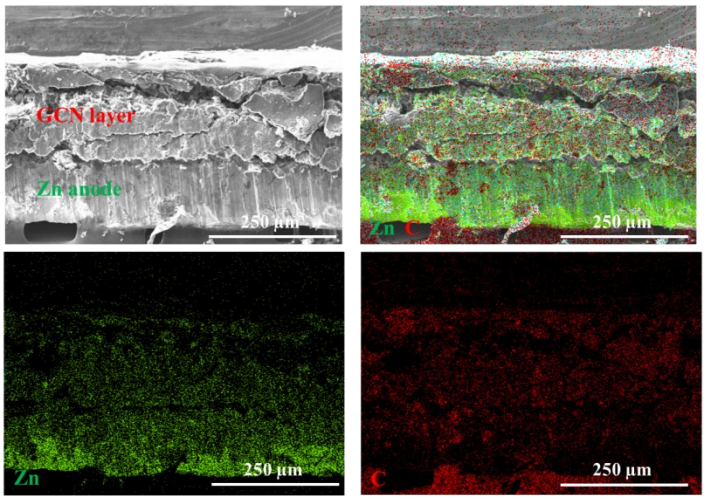

Figure S13. SEM and the corresponding EDS mapping images of CNG/Zn after 15 mins deposition.

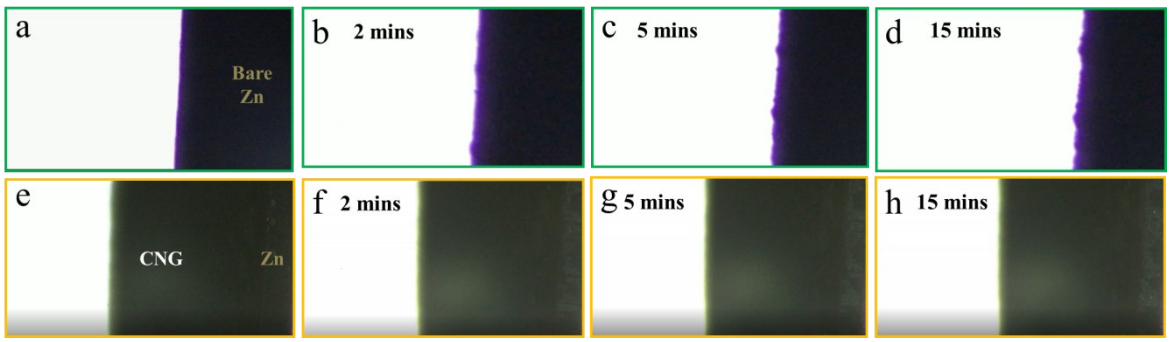

Figure S14. Operando optical observations of Zn depositions of bare Zn anode (a-d) and CNG/Zn anode (e-h).

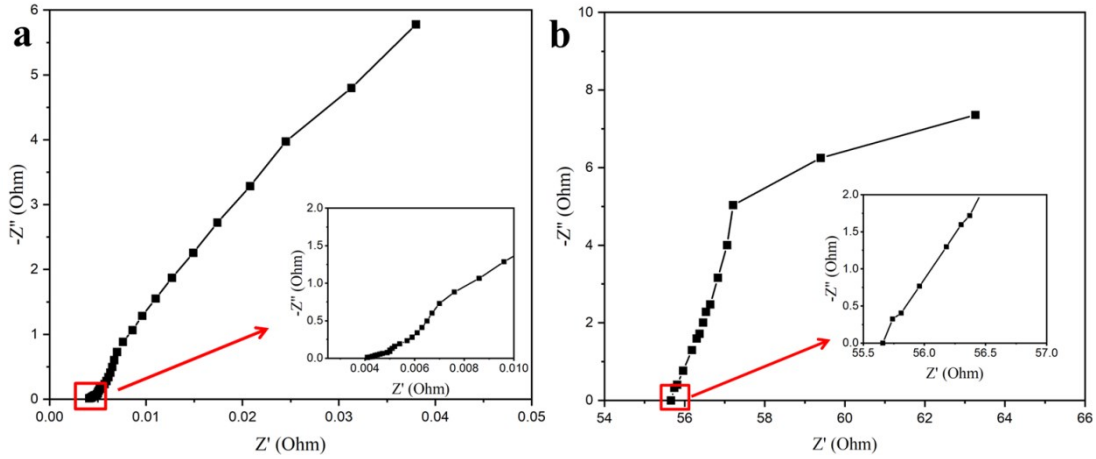

Figure S15. The EIS curves of (a) bare Zn foil and (b) CNG membrane. Here, the thickness (l) of bare Zn foil and CNG membrane is about 18 μm and 52.5 μm, respectively. Effective area (S) of sample is about 1 cm^{-2}, and resistance of the sample is R. The conductivity (σ) calculated using the following equation: $\sigma = l/(R \times S)$. The calculated conductivity values of bare Zn foil and CNG membrane are 0.439 S cm^{-1} and 9.43×10^{-5} S cm^{-1}, respectively.

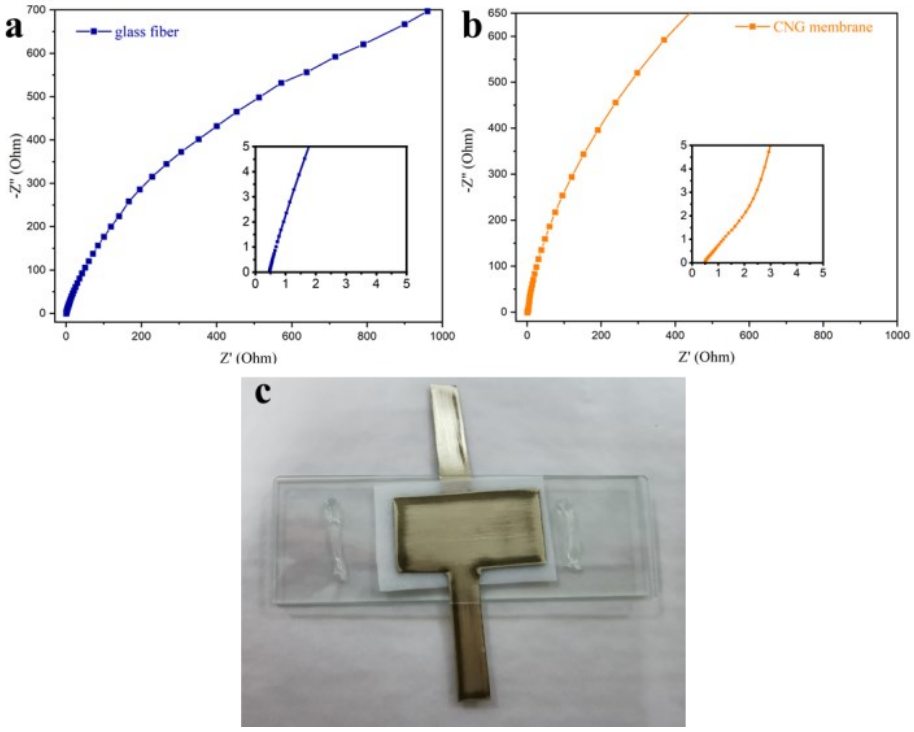

Figure S16. Nyquist plots tested at open circuit voltage (OCV) over the frequency range of 100 kHz to 0.01 Hz. (a) Cu/Cu cell with GF as separator. (b) Cu-CNG/Cu-CNG cell with GF separator. (c) Photograph of test device.

The ionic conductivity of CNG membrane was tested using Cu foil as blocking electrode (Figure S16c). Two Ti foils with CNG layer were fixed in a glass slide, where the wetted glass fiber (GF) separator (~280 μm, 3M $ZnSO_4$ electrolyte) was placed in between. The ionic conductivity of the CNG membrane was evaluated according to the following equation:

$$\sigma = \frac{L}{R_b S}$$

where R_b represents the resistance according to the EIS measurement, L represents the thickness of the CNG membrane (52.5 μm), and S is the contact area (3 cm^2). The testing was conducted at the temperature of 25 °C. Similarly, the ionic conductivity of GF separator could be tested by Cu/Cu cell with GF separator (Figure S16a), R_b (GF) ≈0.44 Ω, σ(GF) ≈2.12 × 10^{-2} S cm^{-1}.

For the CNG membrane, R_b (CNG) ≈0.50 Ω -0.44 Ω =0.06 Ω (Figure S16b), σ(CNG) ≈2.92 × 10^{-2} S cm^{-1}.

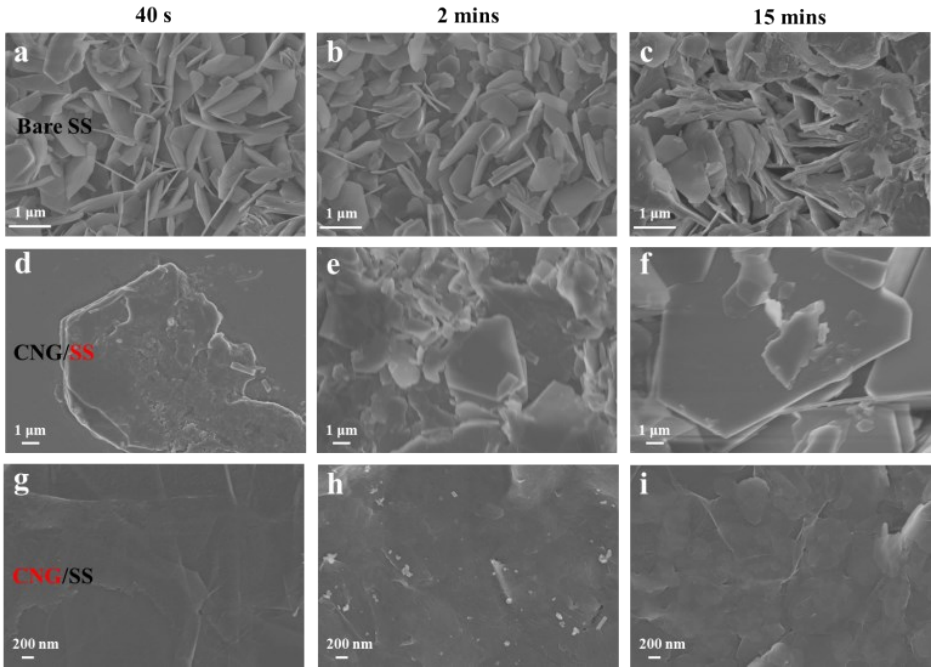

Figure S17. SEM image of Zn deposits on CNG/SS anode and bare SS anode after deposition 40 s, 2 mins, and 15 mins, respectively. Current density, J = 4 mA/cm^2. (a-c) Bare SS anode, (d-f) SS anode protected by CNG layer, (g-i) the CNG layer on the SS anode surface.

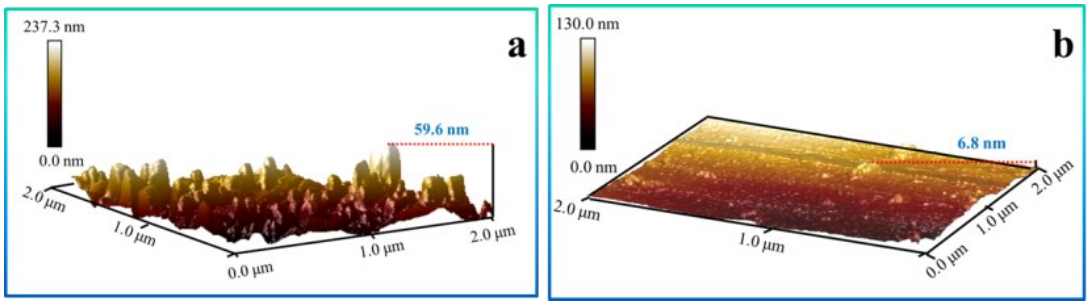

Figure S18. AFM images of (a) bare SS, and (b) CNG/SS anode after 15 mins Zn plating process.

Figure S19. Test device for $ZnSO_4$ permeability.

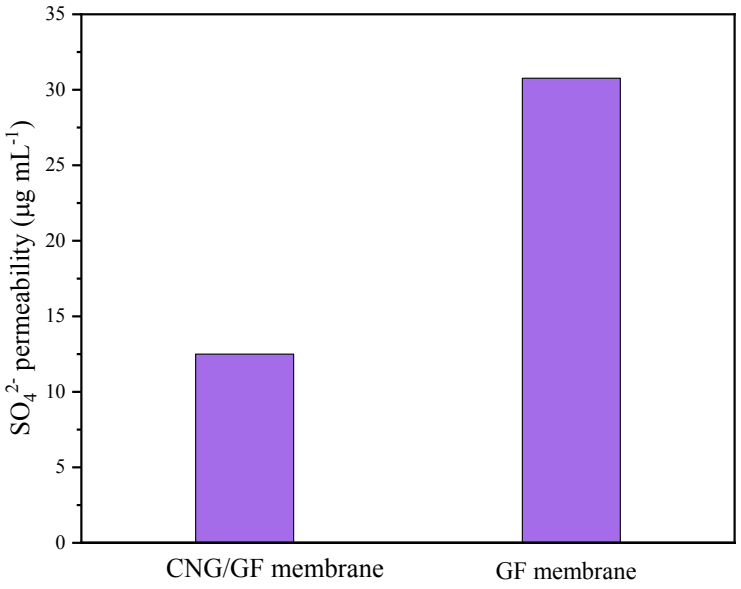

Figure S20. SO_4^{2-} permeability of CNG/GF and GF membrane.

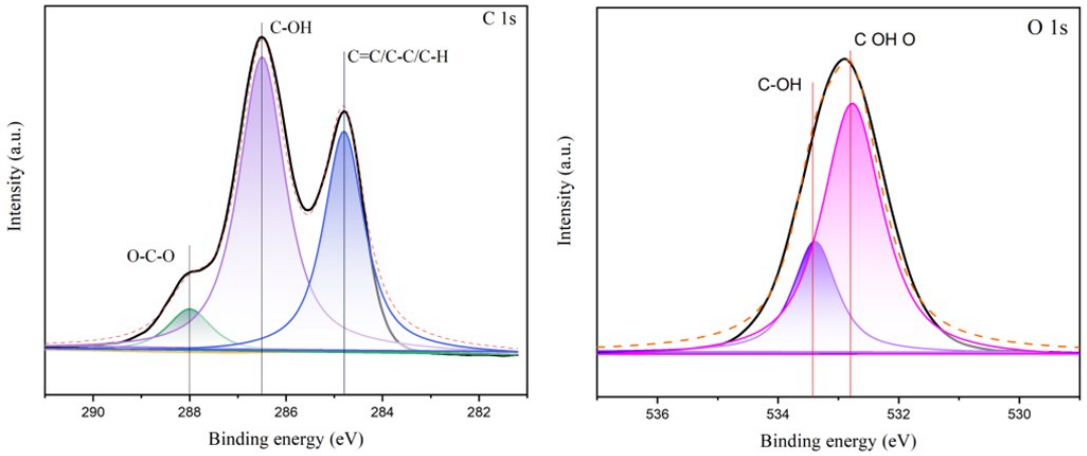

Figure S21. XPS analysis of CNG layer, showing the high-resolution C 1s spectrum and the high-resolution O 1s spectrum.

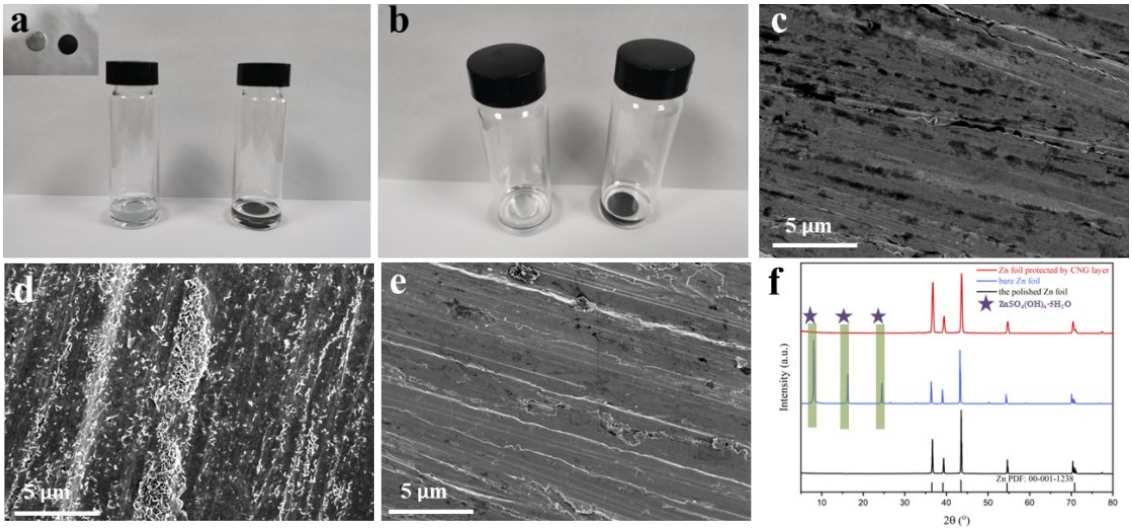

Figure S22. The stability of Zn metal in 3M $ZnSO_4$ electrolyte. (a) bare Zn foil and (b) the protected Zn foil by CNG membrane. SEM image of (c) the polished Zn foil, (d) soaked bare Zn foil and (e) soaked Zn foil protected by CNG membrane. (f) XRD patterns of Zn foils before/after soaking in the electrolyte.

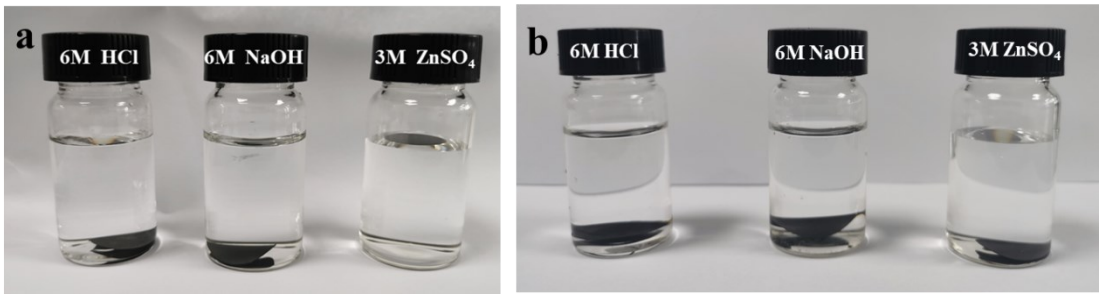

Figure S23. (a) Macroscopic morphologies of CNG membrane in different solution and (b) their changes 90 days later.

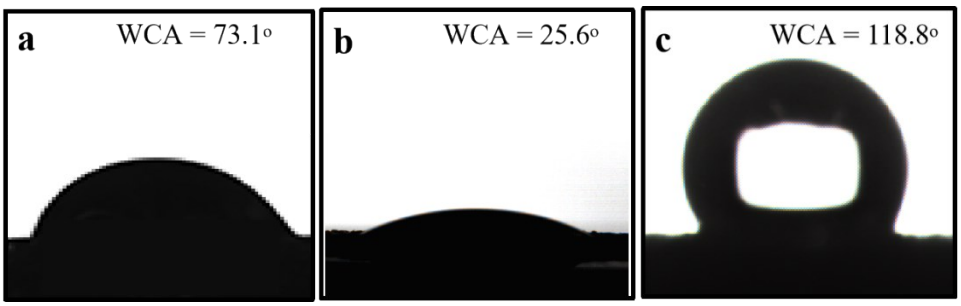

Figure S24. WCAs of (a) bare Zn foil, (b) CNG membrane and (c) CNG membrane after heat-treated in Ar atmosphere at 900 ℃.

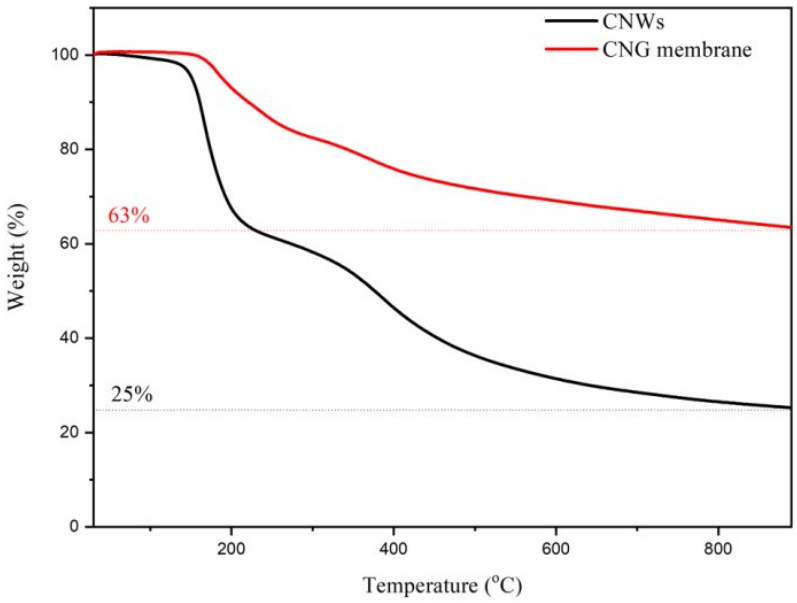

Figure S25. The TG curves of CNWs and CNG membrane.

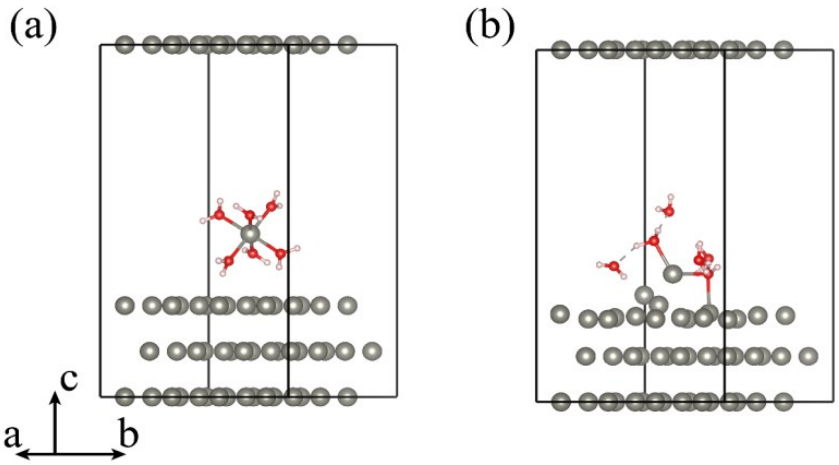

Figure S26. The MD simulation of desolvation behavior of the $[Zn(H_2O)_6]^{2+}$ on the bare Zn anode.

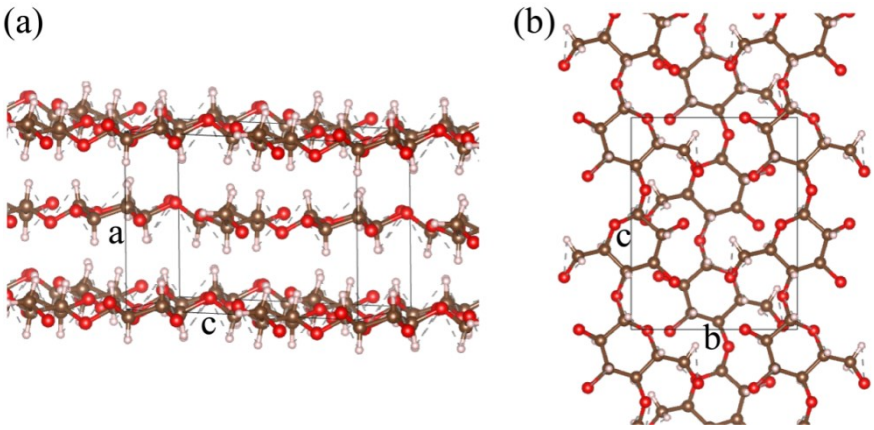

Figure S27. The side view(a) and top view(b) for the crystal structure of I_β cellulose. The dashed lines are H-bonds and the black box is the unite cell.

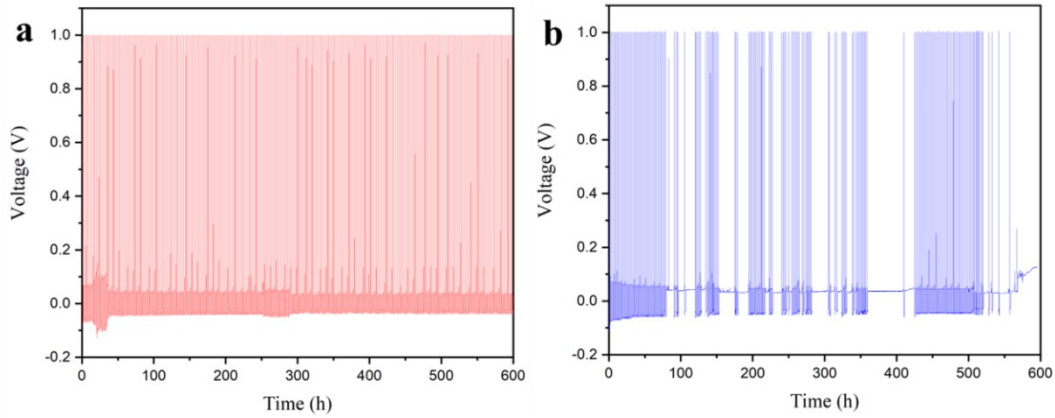

Figure S28. Zn plating/striping curves of (a) CNG/Cu ¦ CNG/Zn asymmetry battery, and (b) Cu ¦ Zn asymmetry battery.

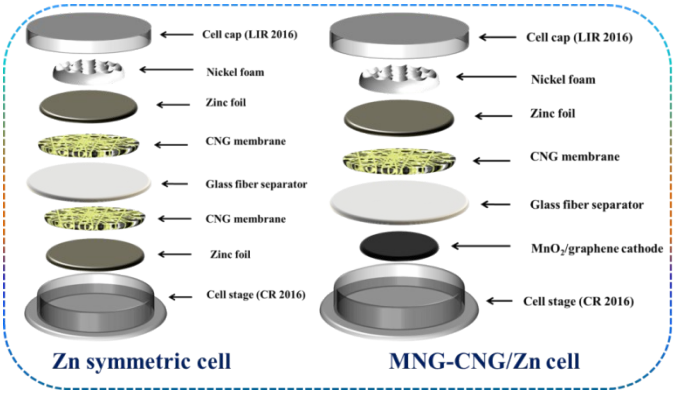

Figure S29. Schematic design of the CNG/Zn symmetric cell and MNG-CNG/Zn cell used in this study.

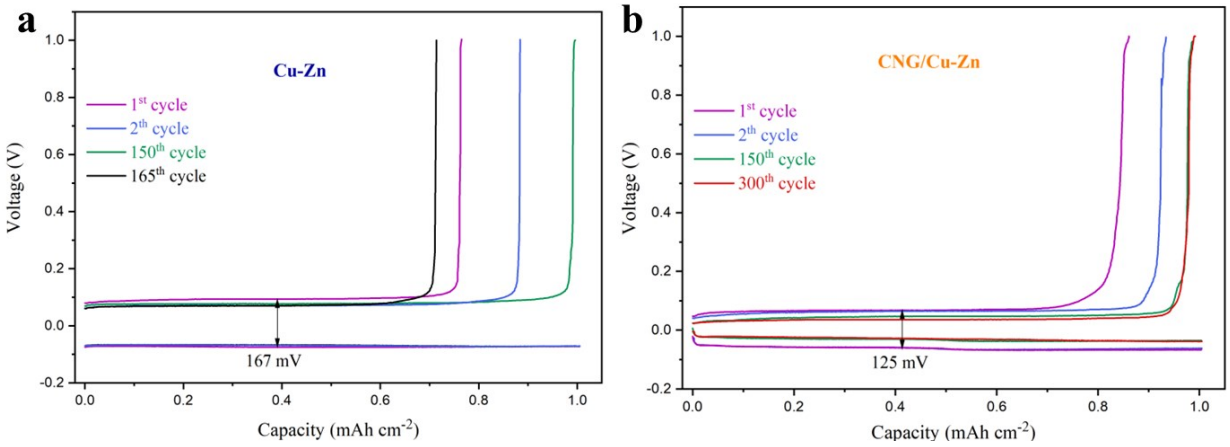

Figure S30. Voltage profiles of (a) the bare Cu-Zn cell and (b) the CNG/Cu-Zn cell at different cycles.

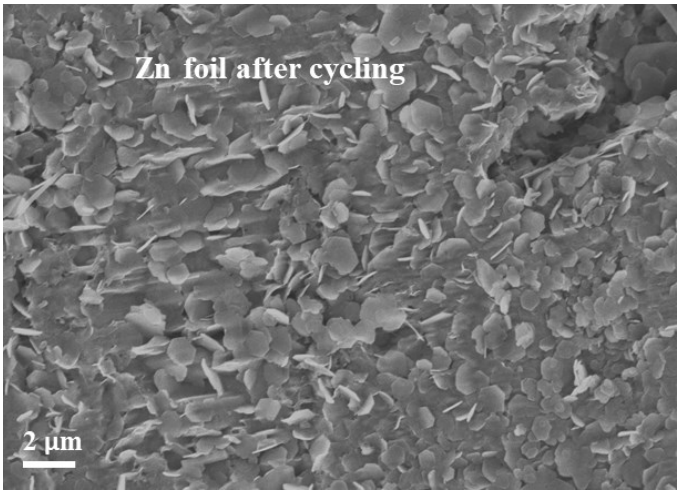

Figure S31. SEM image of cycled bare Zn foil after stripping/plating 200h.

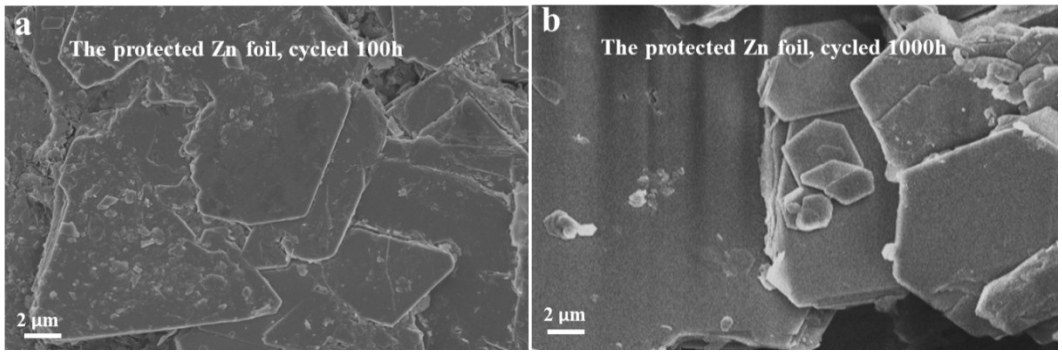

Figure S32. SEM images of cycled Zn anode protected by CNG interface layer after stripping/plating (a) 200h and (b) 1000h, respectively.

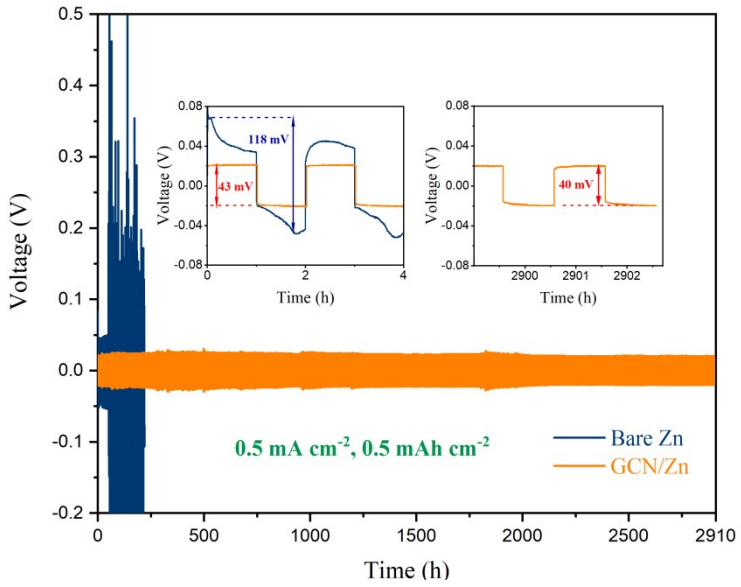

Figure S33. Typical GCD profiles of Zn symmetric cell with/without CNG layer at a current density of 0.5 mA cm^{-2}.

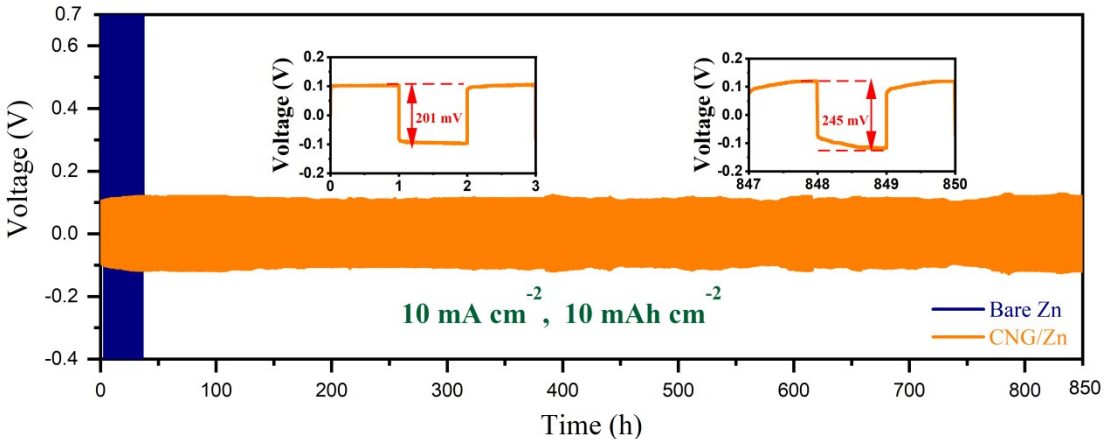

Figure S34. Typical GCD profiles of Zn symmetric cell with/without CNG layer with 10 mAh cm^{-2} at a current density of 10 mA cm^{-2}.

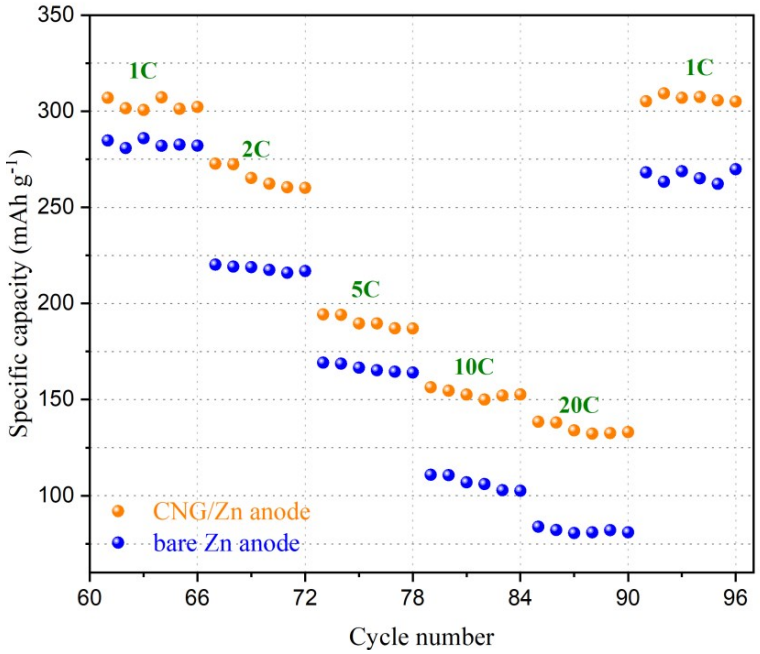

Figure S35. Rater performance of CNG/Zn anode and bare Zn anode.

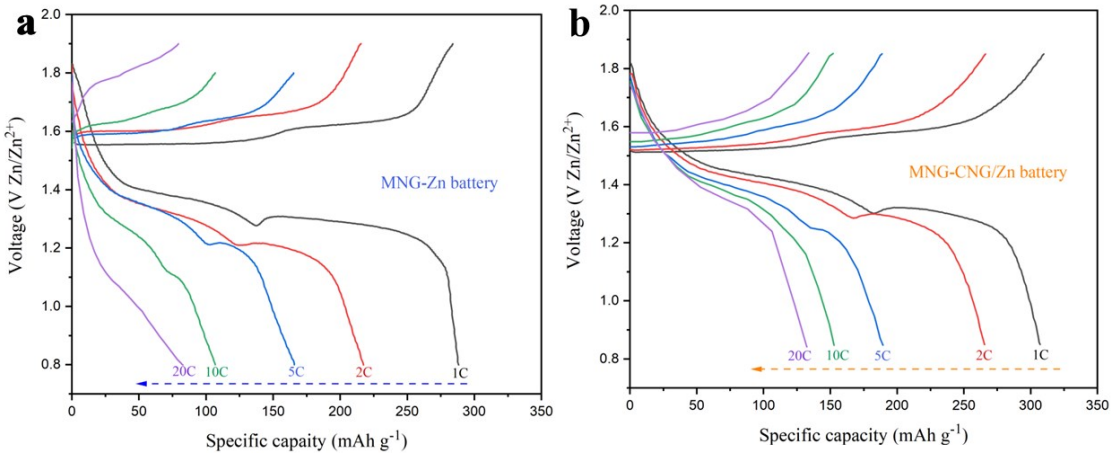

Figure S36. Galvanostatic charge/discharge curves of (a) MNG-Zn battery and (b) MNG-CNG/Zn battery at varying C rates.

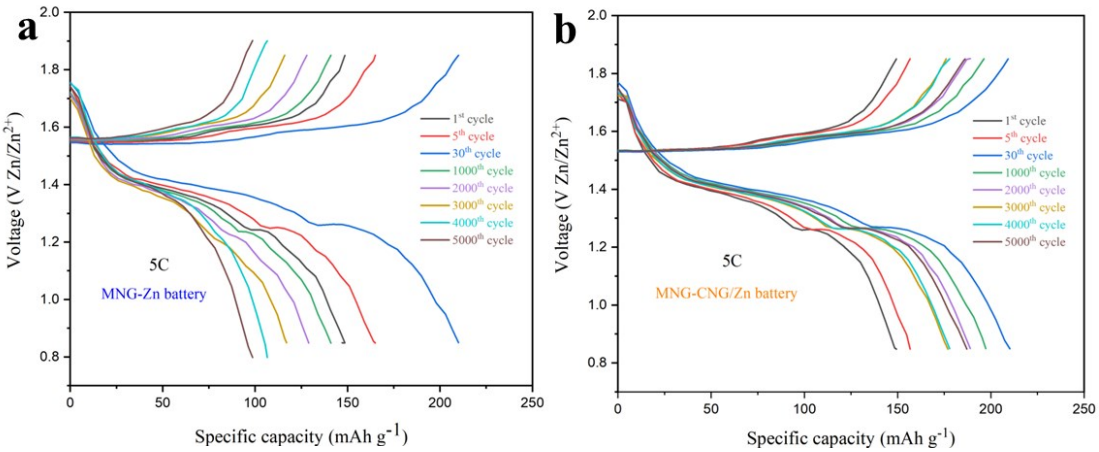

Figure S37. Galvanostatic charge/discharge curves of (a) MNG-Zn battery and (b) MNG-CNG/Zn battery at different cycles.

Table S1. The mass parameters of CNG membranes ($m_{graphene}$:m_{CNWs}=1:1).

Sample	CNG-1	CNG-2	CNG-3
$m_{graphene}$(mg)	60	90	120
thickness(μm)	13.6	40.3	52.5

Table S2. The mass parameters of CNG membranes ($m_{graphene}$ = 120 mg).

Sample	CNG-4	CNG-3	CNG-5
$m_{graphene}$(mg)	120	120	120
M_{CNWs} (mg)	240	120	60

Table S3. Zeta potential (mV) of CNG membrane (m_{GN}:m_{CNWs}=1:1) tested for three times.

Sample	**Test one**	**Test two**	**Test three**	**Average**
CNG	-24.5	-24.6	-24.5	-24.5

Table S4 Performance comparison of Zn symmetric cell of this work and other reported works

Anode Materials	Voltage Hysteresis	Life Span	Ref.
MOF-PVDF/Zn	90 mV (1 mA cm^{-2})	500h (1 mA cm^{-2} 0.5 mAh cm^{-2})	[10]
PBI@Cu/Zn	70 mV (10 mA cm^{-2})	300h (10 mA cm^{-2} 1 mAh cm^{-2})	[11]
ZnS@Zn	98 mV (2 mA cm^{-2})	1100h (2 mA cm^{-2} 2 mAh cm^{-2})	[12]
Lignin@Nafion/Zn	82 mV (0.2 mA cm^{-2})	376h (0.2 mA cm^{-2})	[13]
100TiO_2@Zn	81.8 mV (1 mA cm^{-2})	150h (1 mA cm^{-2} 1 mAh cm^{-2})	[14]
PVB/Zn	108.5 mV (0.5 mA cm^{-2})	2200h (0.5 mA cm^{-2} 0.5 mAh cm^{-2})	[15]
Zn@C	35 mV (1 mA cm^{-2})	200h (1 mA cm^{-2} 1 mAh cm^{-2})	[16]
rGO@Zn	35 mV (0.2 mA cm^{-2})	2000h (0.2 mA cm^{-2} 0.2 mAh cm^{-2})	[17]
Nano-$CaCO_3$/Zn	80 mV (0.25 mA cm^{-2})	836h (0.25 mA cm^{-2} 0.05 mAh cm^{-2})	[18]
HsGDY/Zn	62 mV (0.5 mA cm^{-2})	2400h (0.5 mA cm^{-2})	[19]
KL/Zn	70 mV (4.4 mA cm^{-2})	800h (4.4 mA cm^{-2} 1.1 mAh cm^{-2})	[20]
AEC/Zn	54 mV (0.885 mA cm^{-2})	2000h (0.885 mA cm^{-2} 0.885 mAh cm^{-2})	[21]
$Zn_{88}Al_{12}$	70 mV (0.5 mA cm^{-2})	2000h (0.5 mA cm^{-2})	[22]
3D ZnO/Zn	42 mV (5 mA cm^{-2})	500h (5 mA cm^{-2} 1.125 mAh cm^{-2})	[23]
ZrO_2/Zn	50 mV (0.25 mA cm^{-2})	3800h (0.25 mA cm^{-2} 0.125 mAh cm^{-2})	[24]
β-PVDF/Zn	110 mV (1.5 mA cm^{-2})	1200h (2 mA cm^{-2} 1 mAh cm^{-2})	[25]
ZIF-8@Zn	58 mV (2 mA cm^{-2})	1200h (2 mA cm^{-2} 1 mAh cm^{-2})	[26]
Cu@Zn	46 mV (1 mA cm^{-2})	1500h (1 mA cm^{-2} 0.5 mAh cm^{-2})	[27]
CNT/Zn	40 mV (2 mA cm^{-2})	200h (2mA cm^{-2} 2 mAh cm^{-2})	[28]
$NaTi_2(PO_4)_3$	50 mV (1 mA cm^{-2})	240h (1 mA cm^{-2} 1 mAh cm^{-2})	[29]
NP Zn-Cu	40 mV (2 mA cm^{-2})	300h (2 mA cm^{-2})	[30]
Al_2O_3@Zn	36.5 mV (1 mA cm^{-2})	500h (1 mA cm^{-2} 1 mAh cm^{-2})	[31]
PiZn	40 mV (4 mA cm^{-2})	300h (4 mA cm^{-2} 2 mAh cm^{-2})	[32]
ZnO HPA/Zn	44.4 mV (0.2 mA cm^{-2})	500h (0.2 mA cm^{-2} 0.2 mAh cm^{-2})	[33]
In@Zn	63 mV (0.2 mA cm^{-2})	1500h (0.2 mA cm^{-2} 0.2 mAh cm^{-2})	[34]
LM/Zn	40 mV (1 mA cm^{-2})	500h (1 mA cm^{-2} 0.5 mAh cm^{-2})	[35]
This work	31 mV (0.25 mA cm^{-2})	5500h (0.25 mA cm^{-2} 0.5 mAh cm^{-2})	

References

[1] P. Hohenberg, W. Kohn, *Phys. Rev.,* **1964**, *136*, B864.

[2] W. Kohn, L. J. Sham, *Phys. Rev.,* **1965**, *140*, A1133.

[3] G. Kresse, J. Hafner, *Phys. Rev. B,* **1993**, *47*, 558.

[4] G. Kresse, J. Furthmüller, *Mater. Sci.*, **1996**, *6*, 15.

[5] P. E. Blöchl, *Phys. Rev. B,* **1994**, *50*, 17953.

[6] J. P. Perdew, K. Burke, M. Ernzerhof, *Phys. Rev. Lett*. **1996**, *77*, 17953.

[7] S. Grimme, J. Antony, S. Ehrlich, and S. Krieg, *J. Chem. Phys.,* **2010**, *132*, 154104.

[8] Y. Nishiyama, J. Sugiyama, H. Chanzy, P. Langan, *J. Am. Chem. Soc.,* **2003**, *125*, 14300.

[9] Y. Nishiyama, P. Langan, H. Chanzy, *J. Am. Chem. Soc*., **2002**, *124*, 9074.

[10] M. Liu, L. Yang, H. Liu, A. Amine, Q. Zhao, Y. Song, J. Yang, K. Wang, F. Pan, ACS Appl. Mater. Interfaces, **2019**, 11, 32046.

[11] Q. Jian, Y. Wan, J. Sun, M. Wu, T. Zhao, J. Mater. Chem. A, 2020, 8, 20175.

[12] J. Hao, B. Li, X. Li, X. Zeng, S. Zhang, F. Yang, S. Liu, D. Li, C. Wu, Z. Guo, Adv. Mater., **2020**, 32, 2003021.

[13] D. Yuan, W. M. Jr., L. Zhang, J. J. Chan, S. Meng, Y. Chen, M. Srinivasan, ChemSusChem, **2019**, 12, 4889 –4900.

[14] K. Zhao, C. Wang, Y. Yu, M. Yan, Q. Wei, P. He, Y. Dong, Z. Zhang, X. Wang, L. Mai, *Adv. Mater. Interfaces,* **2018**, *5*, 1800848.

[15] J. Hao, X. Li, S. Zhang, F. Yang, X. Zeng, Sh. Zhang, G. Bo, Ch. Wang, Z. Guo, Adv. Funct. Mater., **2020**, 30, 2001263.

[16] W. Li, K. Wang, M. Zhou, H. Zhan, S. Cheng, K. Jiang, ACS Appl. Mater. Interfaces, **2018**, 10, 22059.

[17] A. Xia, X. Pu, Y. Tao, H. Liu, Y. Wang, Appl. Surf. Sci., 2019, 481, 852.

[18] L. Kang, M. Cui, F. Jiang, Y. Gao, H. Luo, J. Liu, W. Liang, C. Zhi, *Adv. Energy Mater.,* 2018, *8*, 1801090.

[19] Q. Yang, Y. Guo, B. Yan, C. Wang, Z. Liu, Z. Huang, Y. Wang, Y. Li, H. Li, L. Song, J. Fan, C. Zhi, Adv. Mater., 2020, 32, 2001755.

[20] C. Deng, X. Xie, J. Han, Y. Tang, J. Gao, C. Liu, X. Shi, J. Zhou, S. Liang, Adv. Funct. Mater., 2020, 30, 2000599.

[21] R. Zhao, Y. Yang, G. Liu, R. Zhu, J. Huang, Z. Chen, Z. Gao, X. Chen, L. Qie, Adv. Funct. Mater., 2021, 31, 2001867.

[22] S. Wang, Q. Ran, R. Yao, H. Shi, Z. Wen, M. Zhao, X. Lang, Q. Jiang, Nat. Commun., 2020, 11, 1634.

[23] X. Xie, S. Liang, J. Gao, S. Guo, J. Guo, C. Wang, G. Xu, X. Wu, G. Chen, J. Zhou, Energy Environ. Sci., 2020, 13, 503.

[24] P. Liang, J. Yi, X. Liu, K. Wu, Z. Wang, J. Cui, Y. Liu, Y. Wang, Y. Xia, J. Zhang, *Adv. Funct. Mater.,* 2020, *30*, 1908528.

[25] L. T. Hieu, S. So, I. T. Kim, J. Hur, Chem. Eng. J., DOI: 10.1016/j.cej.2021.128584.

[26] X. Liu, F. Yang, W. Xu, Y. Zeng, J. He, X. Lu, Adv. Sci., 2020, 7, 2002173.

[27] Z. Cai , Y. Ou , J. Wang , R. Xiao , L. Fu , Z. Yuan, R. Zhan, Y.g Sun, Energy Storage Mater., 2020, 27, 205.

[28] Y. Zeng, X. Zhang, R. Qin, X. Liu, P. Fang, D. Zheng, Y. Tong, X. Lu, Adv. Mater., 2019, 31, 1903675.

[29] M. Liu, J. Cai, H. Ao, Z. Hou, Y. Zhu, Y. Qian, Adv. Funct. Mater., 2020, 30, 2004885.

[30] B. Liu, S. Wang, Z. Wang, H. Lei, Z. Chen, W. Mai, *Small,* **2020**, *16*, 2001323.

[31] H. He, H. Tong, X. Song, X. Song, J. Liu, J. Mater. Chem. A, 2020, 8, 7836.

[32] M. Zhu, J. Hu, Q. Lu, H. Dong, D. D. Karnaushenko, C. Becker, D. Karnaushenko, Y. Li, H. Tang, Z. Qu, J. Ge, O. G. Schmidt, Adv. Mater., 2021, 2007497.

[33] J. Y. Kim, G. Liu, G. Y. Shim, H. Kim, J. K. Lee, Adv. Funct. Mater., 2020, 30, 2004210.

[34] D. Han, S. Wu, S. Zhang, Y. Deng, C. Cui, L. Zhang, Y. Long, H. Li, Y. Tao, Z. Weng, Q. –H. Yang, F. Kang, Small, 2020, 16, 2001736.

[35] H. Jia, Z. Wang, M. Dirican, S. Qiu, C. –Y. Chan, S. Fu, B. Fei, X. Zhang, J. Mater. Chen. A, 2021, DOI: 10.1039/D0TA11828A.